The Meteoritical Society

Meteoritics & Planetary Science 52, Nr 5, 937–948 (2017)
doi: 10.1111/maps.12842

Petrology, mineralogy, porosity, and cosmic-ray exposure history of Huaxi ordinary chondrite

Shijie LI[1], Shijie WANG[2,*], Ingo LEYA[3], Yang LI[1], Xiongyao LI[1], and Thomas SMITH[3]

[1]Center for Lunar and Planetary Sciences, Institute of Geochemistry, Chinese Academy of Sciences, Guiyang 550081, China
[2]State Key Laboratory of Environmental Geochemistry, Institute of Geochemistry, Chinese Academy of Sciences, Guiyang 550081, China
[3]Physikalisches Institut, Universität Bern, Switzerland
[*]Corresponding author. E-mail: wangshijie@vip.skleg.cn

(Received 30 November 2016; revision accepted 11 January 2017)

Abstract–A meteorite fall was heard and collected on July 13, 2010 at about 18:00 (local time) in the Shibanjing village of the Huaxi district of Guiyang, Guizhou province, China. The total mass of the fall is estimated to be at least 1.6 kg; some fragments are missing. The meteorite consists mainly of olivine, low-Ca pyroxene, high-Ca pyroxene, plagioclase, kamacite, taenite, and troilite. Minor phases include chromite and apatite. Various textural types of chondrules exist in this meteorite: most chondrule textures can be easily defined. The grain sizes of secondary plagioclase in this meteorite range from 2 to 50 μm. The chemical composition of olivine and low-Ca pyroxene are uniform; Fa in olivine and Fs in low-Ca pyroxene are, respectively, 19.6 ± 0.2 and 17.0 ± 0.3 (mole%). Huaxi has been classified as an H5 ordinary chondrite, with a shock grade S2, and weathering W0. The weak shock features, rare fractures, and the high porosity (17.6%) indicates that Huaxi is a less compacted meteorite. The preatmospheric radius of Huaxi is ~11 cm, corresponding to ~21 kg. The meteorite experienced a relatively short cosmic-ray exposure of about 1.6 ± 0.1 Ma. The ^{4}He and ^{40}Ar retention ages are older than 4.6 Ga implying that Huaxi did not degas after thermal metamorphism on its parent body.

INTRODUCTION

A fist-size stone fell in a farmyard in Shiban Village, Huaxi District, Guiyang City, Guizhou province, China at about 18:00 (local time) on July 13, 2010 (Fig. 1). The owner of the farmyard (Fig. 2a) heard the sound of the stone falling accompanied by a heavy thudding noise against the slate floor. The stone created a small crater (geographic coordinates 26°27′52.88″ N, 106°37′56.68″ E) in the carbonate slate with radial fractures in the northeast rim (Fig. 2b). All fragments of the stone were collected in a corner of the northeast wall of the farmyard. Both findings indicate a flight direction southwest-northeast. The stone was broken into more than four fragments after the impact (Fig. 3). Each of the four collected fragments is partly covered by fusion crust. The total mass of all four fragments is ~1600 g. The biggest fragment has a mass of ~1200 g and the three smaller pieces have a total mass of ~400 g. One or more fragment(s), with a total mass of ~100 g, is unaccounted for; it may have bounced into the cornfield next to the northern wall of the farmyard. The meteorite was named Huaxi in the Meteorite Bulletin No. 100 (Ruzicka et al. 2014). The Huaxi meteorite is the fourth meteorite fall in the Guizhou province, China, after the fall or find of Anlong, Guizhou, and Qingzhen.

SAMPLE AND ANALYTICAL TECHNIQUES

The noble gas measurements were performed at the University of Bern, Switzerland. Other measurements were carried out at the Institute of Geochemistry, Chinese Academy of Sciences, Guiyang, China.

A polished section and one double polished thin section (30 μm thickness) of Huaxi were prepared for petrographic investigations and mineral chemical composition analysis. For investigating the pores, we

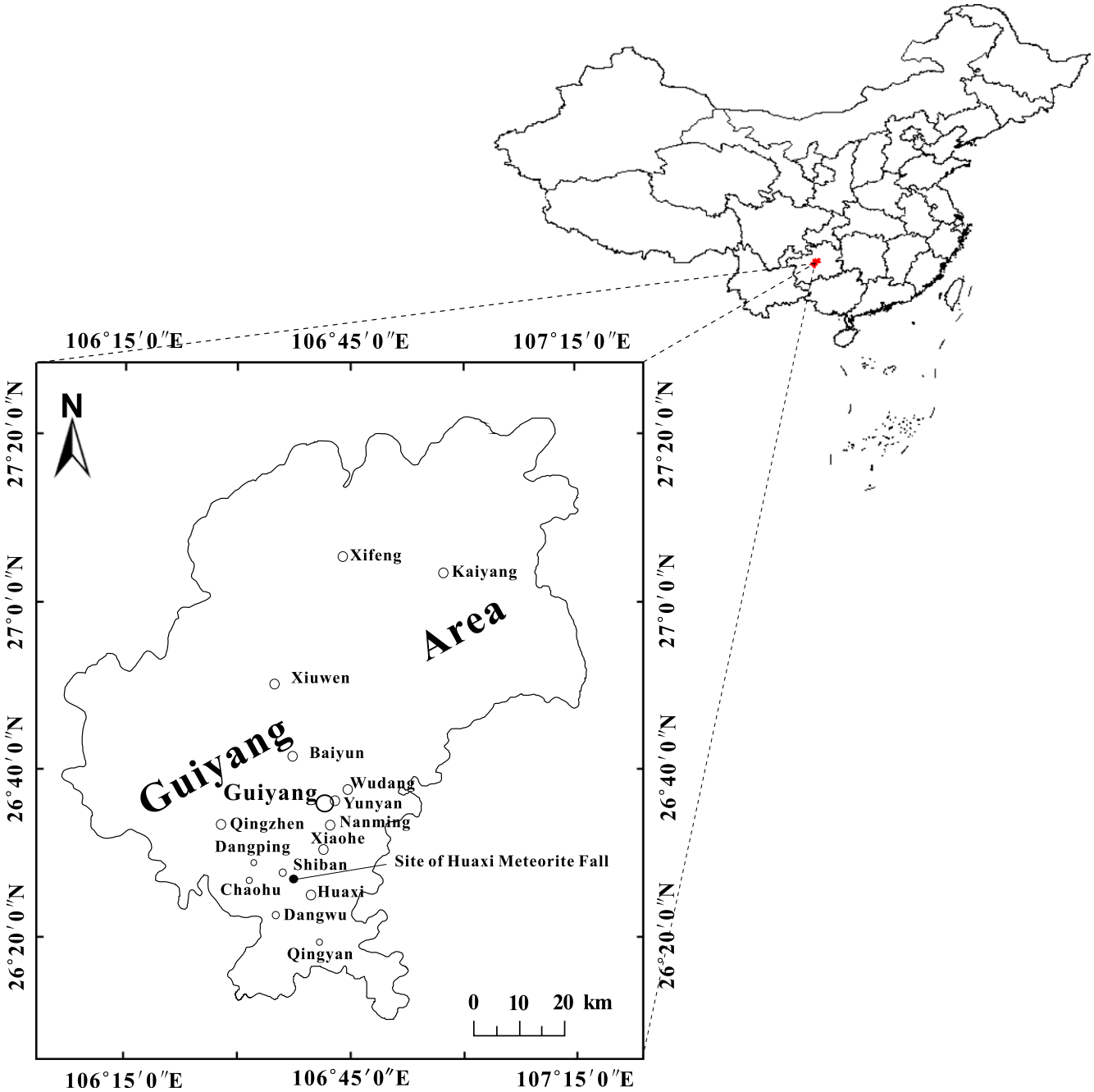

Fig. 1. Map of the Huaxi meteorite fall area. (Color figure can be viewed at wileyonlinelibrary.com.)

also prepared a slice sample. Petrographic investigations were performed with a JEOL JSM-6610LV scanning electron microscope (SEM) equipped with an EDAX energy dispersive X-ray spectrometry (EDS) and a Scios-FIB field emission scanning electron microscope. The shock stage was determined using the double polished thin section and an OLYMPUS-BX51 polarizing microscope in transmitted light. For determining the major element composition of olivine and low-Ca pyroxene, we used the EPMA-1600 electron microprobe with an acceleration voltage of 15 kV and a beam current of 20 nA. Silicates (olivine for Mg and Fe; plagioclase for Al, Si, and Ca; pyrope garnet for Ti, Cr, and Mn) were used as standards. We applied the standard ZAF-correction procedure for data reduction. For measuring the whole rock chemical composition we prepared a fine powder of 50 mg, which was digested with a mixture of HF and HNO_3. The concentrations of

Fig. 2. The place where Huaxi landed. a) The farmyard where the Huaxi meteorite fell. b) The small crater made by the impact of the Huaxi meteorite. (Color figure can be viewed at wileyonlinelibrary.com.)

Fig. 3. The main mass and three fragments of the Huaxi meteorite. (Color figure can be viewed at wileyonlinelibrary.com.)

Na, K, Ca, and Mn were analyzed by a Vista MPX ICP-OES. Magnesium, Fe, Co, and Ni were measured by a PinAAcle 900F ICP-AAS; other trace element concentrations were measured using an ELAN DRC-e ICP-MS. Cobalt, Ni, and Sr were measured on both ICP-AAS and ICP-MS. Five platinum group elements, including Ru, Rh, Pd, Pt, and Ir, were measured with a Finnigan MAT ELEMENT magnetic sector ICP-MS using a 200 mg aliquot of the solution and applying the method described in Qi et al. (2003, 2011). Four fragments of Huaxi with masses of 2.29, 3.82, 2.84, and 3.26 g were used for the determination of densities and porosities with a Micro-ultrapyc 1200e ideal gas pycnometer and applying the method developed by Li et al. (2012). The light noble gases were measured on two small fragments with masses of 55.62 and 57.09 mg. The selected fragments were located ~2 mm and 1 cm below the fusion crust, respectively. The isotopic concentrations of He, Ne, and Ar have been measured by noble gas mass spectrometry at the University of Bern following standard procedures (e.g., Ammon et al. 2008; Leya et al. 2013). Briefly, after cleaning the samples with ethanol they were wrapped in 9 cm^2 aluminum foils and were loaded in an all metal sample chamber. The sample chamber was evacuated and was then heated together with the samples at approximately 80 °C for 3 days to release terrestrial gas contamination. Noble gases were extracted in a single temperature step at about 1700 °C for 45 min. The extracted gases were cleaned on various getters (SAES®) working in the temperature range between room temperature and 280 °C. After cleaning, Ar was trapped on an activated charcoal held at the temperature of liquid N_2 and the remaining He and Ne fraction was further purified and expanded into the inlet of a 90 ° sector field mass spectrometer with a radius of 10 cm. After further purification, the Ar fraction was expanded into a self-made tandem mass spectrometer.

RESULTS

Petrography

Huaxi is a typical chondrite (Fig. 4) containing a variety of chondrule types: porphyritic pyroxene (Fig. 5a), porphyritic olivine (Fig. 5b), porphyritic olivine and pyroxene (Fig. 5c), barred olivine (Fig. 5d),

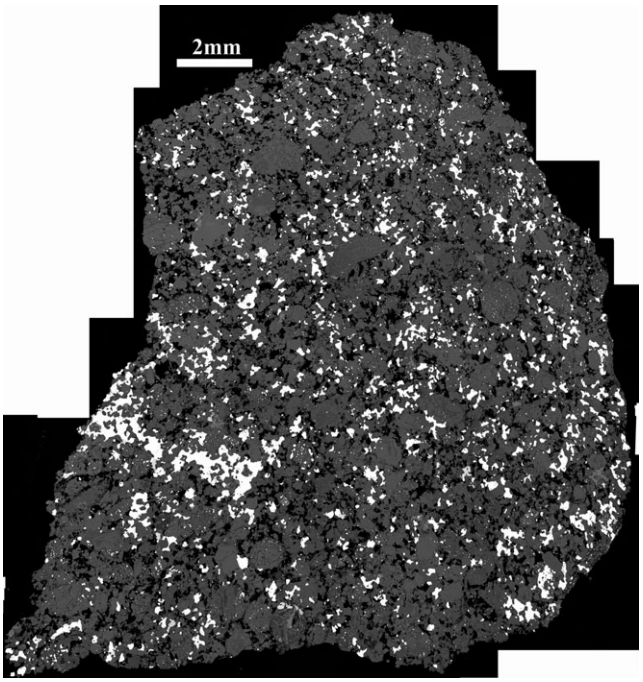

Fig. 4. The BSE image of a polished thin section of the Huaxi meteorite. The significant characteristic of this meteorite is the high porosity.

cryptocrystalline chondrules (Fig. 5e), compound chondrules (Fig. 5f), and Cr and Al rich chondrules (Figs. 5g and 5h). The apparent diameters of distinguishable chondrules range from ~200 to ~1500 μm; the mean diameter is ~500 μm. Matrix material in Huaxi is significantly recrystallized and contains secondary plagioclases with grain sizes ranging from 2 to 50 μm. Huaxi is petrographic grade 5 according to the criteria of Van Schmus and Wood (1967). The meteorite is mainly composed of low-Ca pyroxene (30 vol%), olivine (27 vol%), plagioclase (12 vol%), Fe-Ni metal (kamacite and taenite, 8 vol%), high-Ca pyroxene (5 vol%), troilite (4 vol%), as well as minor apatite and chromite (<1 vol%). The most significant characteristic of this meteorite is the porous texture (Figs. 4 and 6a), which represents about 14 vol% of the analyzed section. A small (~10 × 30 μm) metal copper (contains 6 wt% Fe and 3 wt% Ni, according to EDS area analysis) grain was observed at a grain boundary between troilite and taenite (Fig. 6b) and plessite was observed in a taenite grain (Fig. 6c). There is no indication of shock veins in any of the fresh surfaces of the hand specimen. In addition, we found no microscopic shock vein in the studied thin sections and polished sections. Most olivine grains show undulatory extinction and we found no olivine grain with planar fractures. These findings indicate that Huaxi is weakly shocked with shock stage S2 based on the criteria described in Stöffler et al. (1991), although a few olivine grains with mosaic extinction can be found in the polished thin sections. Fractures in all mineral grains are very rare, indicating that the meteorite is only weakly shocked. Since Huaxi was collected within 10 minutes after its fall, it is very fresh and has therefore a weathering degree W0 according to the classification scheme by Wlotzka (1993).

Mineral Composition

We analyzed the chemical composition of olivine and low-Ca pyroxene in a thin section using EPMA. Ten olivine and 12 low-Ca pyroxene grains were randomly selected and measured. The data are given in Table 1. The fayalite content of the 10 olivine grains varies between 19.3 and 20.1 mole% with an average value of 19.6 ± 0.2 mole%. EDS analysis indicated that there is no chemical zoning in the studied olivine grains. Low-Ca pyroxene is the most abundant mineral in Huaxi. The ferrosilite content in the 12 selected low-Ca pyroxene grains ranges from 16.4 to 17.5 mole% with an average value of 17.0 ± 0.3 mole%. The wollastonite content in low-Ca pyroxene ranges from 1.6 to 2.0 mole% (the average value of 12 grains is 1.8 ± 0.1 mole%). The uniform chemical composition of olivine (PMD value of Fa is 1.3) in Huaxi indicates that this meteorite is an equilibrated chondrite. The fayalite and ferrosilite content in olivine and low-Ca pyroxene, respectively, are in the range of previous measurements for H chondritse (i.e., Fa 16.9–20.4 mole%, Fs 15.7–18.1 mole%, Keil and Fredriksson 1964; Gomes and Keil 1980).

Densities and Porosity

In contrast with many other ordinary chondrite types, the fusion crust of Huaxi is easy to remove. Four small fragments with masses of 2.29, 3.83, 2.84, and 3.26 g were selected for density and porosity determination. The results are compiled in Table 2. The measured bulk densities range from 3.11 to 3.29 g cm^{-3}, the weighted average bulk density is 3.21 g cm^{-3}. The grain densities of the four selected fragments range from 3.82 to 3.98 g cm^{-3}. The weighted average grain density of 3.89 g cm^{-3} is in the range typical for H-chondrites, i.e., 3.53–4.15 g cm^{-3} (Consolmagno et al. 2006).

The porosities of the four fragments measured by ideal gas pycnometry range from 16.5 to 18.7% with a weighted mean of 17.6%. A high porosity is also indicated by the BSE images of the prepared sections, which shows that pore space is usually larger than the space occupied by metal plus troilite (Fig. 6a). A high porosity is also indicated by phase analysis with EDS,

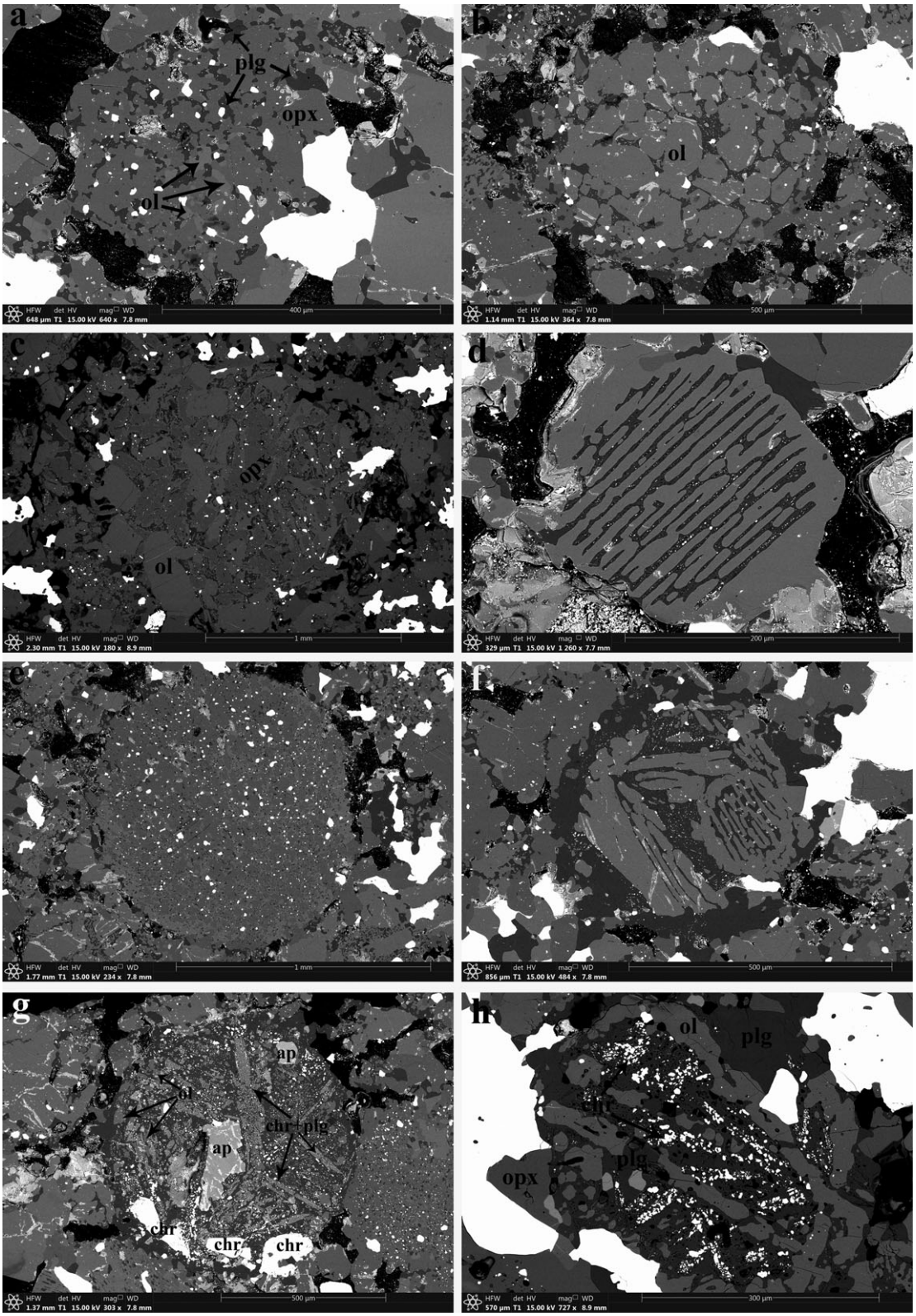

Fig. 5. BSE images of chondrules from the Huaxi meteorite. a) Porphyritic pyroxene chondrule. b) Porphyritic olivine chondrule. c) Porphyritic olivine-pyroxene chondrule. d) Barred olivine chondrule. e) Cryptocrystalline chondrule. f) Compound chondrule. g) Al,Cr-rich chondrule (with apatite in the chondrule). h) Al,Cr-rich chondrule. Acronyms: olivine (ol), low-Ca pyroxene (opx), plagioclase (plg), apatite (ap), and chromite (chr).

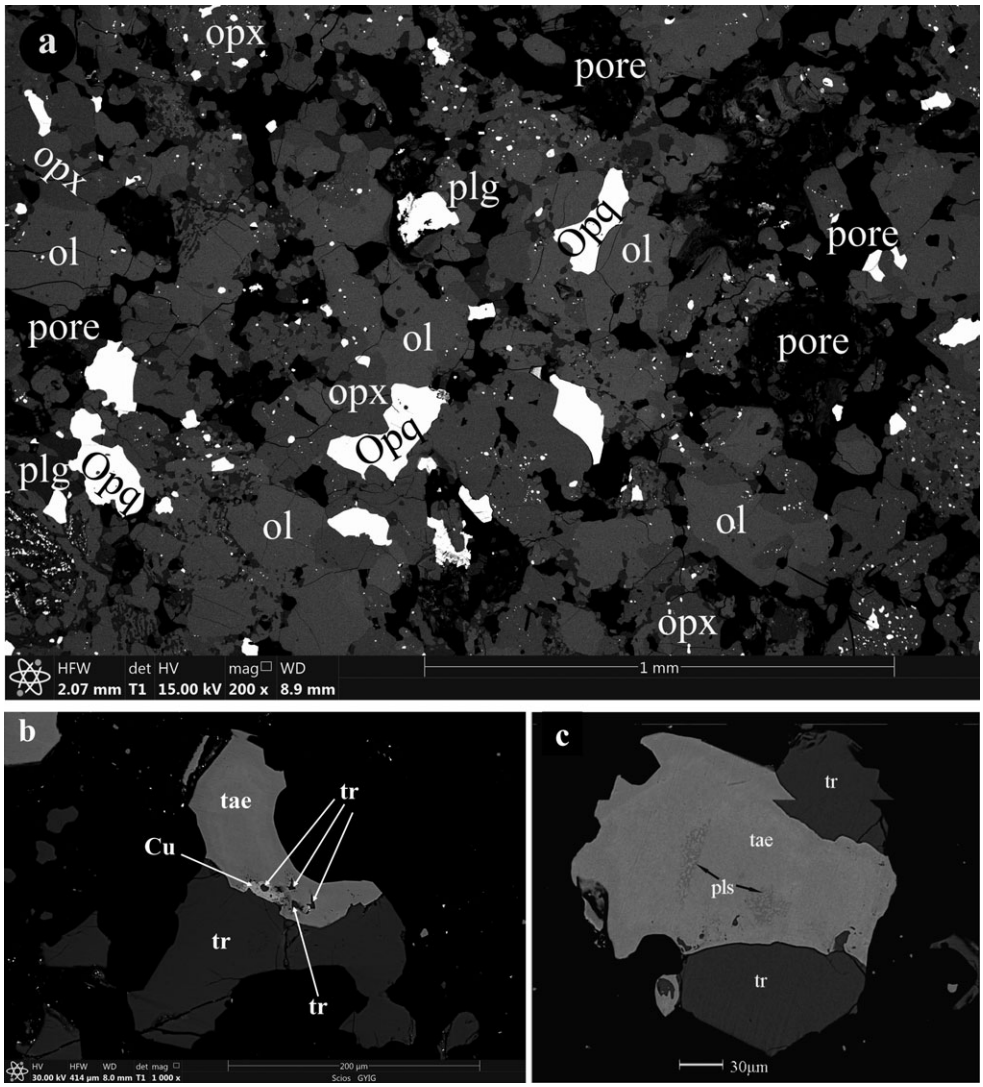

Fig. 6. BSE images of petrologic structures and opaque minerals in Huaxi. a) Chondrules in Huaxi. b) Occurrence of copper. c) Plessite in taenite. Acronyms: olivine (ol), low-Ca pyroxene (opx), plagioclase (plg), opaque minerals (Opq). The Opq include kamacite, taenite (tae), plessite (pls), troilite (tr), copper (Cu), and chromite.

though the EDS analyzed data give a slightly lower porosity of ~14%. This is likely due to the occurrence of tiny pores and fractures that are undetectable under limited magnification (under ×400) during phase analysis. The pores in Huaxi are mainly intergranular or are present as porosity halos in rims around chondrules (Figs. 6, 7, and 8). Low contrast images taken from the polished slice also confirm that this meteorite is porous (Fig. 7a). The walls of the pores consist of minerals with subhedron or/and isiomorphic crystals (Fig. 7b), which indicates that the pore structure formed during thermal metamorphism on the parent asteroid. The distribution of pores in Huaxi is similar to those in the Miller H5 ordinary chondrite i.e., 20.0%, which is considered as an incompletely compacted meteorite (Sasso et al. 2009; Friedrich et al. 2014). The average porosity of ordinary chondrite falls is ~9% (Consolmagno et al. 2008; Macke 2010). Compared to average ordinary chondrite falls, Huaxi has a much higher porosity. It may be significant that most high porosity values occur in type 5 meteorites: Miller (H5, porosity of 20%), NWA 2380 (L5, porosity of 18.7%), Sahara 98034 (H5, porosity of 16.1%), Baszkówka (L5, porosity of 18.4–19.4%), Zaoyang (H5, porosity of 17.5%), and Jinju (H5, porosity of 19.5%) (Sasso et al. 2009; Li et al. 2012; Friedrich et al. 2014; Choi et al. 2015). At this time, it is unknown whether this pattern indicates a significant process or whether it is a coincidence. From the comparison with the Miller chondrite we conclude that Huaxi is most likely also an incompletely compacted chondrite.

Table 1. Representative electron microprobe analyses of olivine and low-Ca pyroxene (wt%).

	SiO_2	TiO_2	Al_2O_3	Cr_2O_3	FeO	MnO	MgO	CaO	Total	Fa/Fs	Wo
Ol-1	38.7	b.d.	0.01	b.d.	18.7	0.47	42.6	0.01	100.5	19.8	–
Ol-2	39.1	b.d.	0.02	b.d.	18.3	0.44	42.3	0.01	100.1	19.5	–
Ol-3	38.2	b.d.	b.d.	0.01	17.9	0.48	42.1	0.02	98.7	19.3	–
Ol-4	38.7	b.d.	b.d.	0.03	18.1	0.42	41.9	0.04	99.2	19.5	–
Ol-5	38.8	b.d.	b.d.	0.02	18.0	0.43	42.0	0.02	99.2	19.4	–
Ol-6	38.0	b.d.	b.d.	0.05	18.3	0.40	42.0	0.02	98.7	19.6	–
Ol-7	38.0	b.d.	b.d.	b.d.	18.1	0.39	41.5	0.01	98.0	19.7	–
Ol-8	39.0	0.06	b.d.	0.23	17.9	0.40	41.9	b.d.	99.4	19.3	–
Ol-9	39.5	b.d.	b.d.	b.d.	17.9	0.46	39.9	0.01	97.8	20.1	–
Ol-10	39.9	b.d.	b.d.	b.d.	18.0	0.41	41.6	0.02	100.0	19.5	–
Pyx-1	56.7	0.21	0.17	0.19	11.4	0.44	30.3	0.91	100.3	17.2	1.8
Pyx-2	57.3	0.19	0.14	0.14	11.2	0.47	30.5	0.84	100.9	16.9	1.6
Pyx-3	56.1	0.23	0.16	0.22	11.5	0.43	30.7	1.01	100.3	17.0	1.9
Pyx-4	57.3	0.23	0.20	0.20	11.3	0.43	29.0	0.98	99.5	17.5	2.0
Pyx-5	57.4	0.21	0.16	0.19	10.9	0.47	30.2	0.91	100.5	16.6	1.8
Pyx-6	56.5	0.15	0.13	0.17	11.2	0.45	30.7	0.92	100.1	16.7	1.8
Pyx-7	55.5	0.20	0.15	0.18	11.5	0.45	30.5	0.96	99.5	17.2	1.8
Pyx-8	56.4	0.22	0.17	0.15	11.5	0.47	30.2	0.98	100.1	17.2	1.9
Pyx-9	56.9	0.14	b.d.	0.17	11.0	0.19	30.2	0.84	99.3	16.6	1.6
Pyx-10	57.2	0.19	0.18	0.19	11.5	0.47	30.4	0.82	101.0	17.2	1.6
Pyx-11	57.4	0.28	0.19	0.19	11.5	0.46	30.0	0.97	101.0	17.3	1.9
Pyx-12	58.8	0.20	0.19	0.18	10.9	0.49	30.5	0.98	102.2	16.4	1.9

The detection limits of MgO, Al_2O_3, CaO, and SiO_2 are all 0.01%; of Cr_2O_3, FeO, and MnO are 0.02%; and of TiO_2 is 0.05%. b.d. = below detection limit.

Table 2. The densities and porosities of four Huaxi fragments.

Sample number	Mass (g)	Bulk density (g cm^{-3})	Grain density (g cm^{-3})	Porosity (%)
1	2.29	3.15	3.83	17.6
2	3.83	3.29	3.98	17.4
3	2.84	3.26	3.90	16.5
4	3.26	3.11	3.82	18.7
Average	–	3.21	3.89	17.6

Errors for densities are less than 0.01 g cm^{-3}, errors for porosity are less than 0.5%. The average has been calculated as a weighted mean.

Bulk Composition

The chemical composition for major and trace elements measured for a whole rock sample is given in Table 3. The element distribution normalized to Mg and CI chondrites is shown in Fig. 8. Also shown are average data for H and L chondrites (Lodders and Fegley 1998). Most of the lithophile elements in Huaxi show an abundance pattern similar to average H and L chondrites. Exceptions are Sc and Cr, which are lower, and Na and La, which are slightly higher than average abundances in H and L chondrites. For the chalcophile elements such as Cu (not shown), Zn, Ga, As, and Sb, the concentrations in Huaxi are very similar to the average composition of H chondrites. The concentration of the chalcophile Ge in Huaxi is higher than the mean concentration in H chondrites (not shown). Most of the siderophile elements (i.e., Fe, Co, Ni, Mo, Ru, and Ir) are significantly higher in Huaxi compared to average abundances in ordinary chondrite, whereas rhodium in Huaxi is lower compared to the average concentration in H chondrites (not shown, 111 ng g^{-1} versus 210 ng g^{-1}). The relatively high concentrations of siderophile elements might mainly be due to a sampling bias. For example, a heterogeneous distribution of Fe-Ni metal can easily be seen in the prepared sections (Fig. 4).

Noble Gas Isotopic Compositions and Concentrations

The concentrations and isotopic ratios of the light noble gases He, Ne, and Ar after blank subtraction and correction for instrumental mass fractionation are listed in Table 4. The measured $^{20}Ne/^{22}Ne$ ratios of the two aliquots are 0.912 and 1.199, indicating that in addition to cosmogenic there is a small trapped contribution. Considering the high petrographic grade for Huaxi (H5) it is unlikely that the trapped component is planetary Ne. To separate the Ne components we assumed cosmogenic and terrestrial compositions for $^{20}Ne/^{22}Ne$ of 0.8 and 9.8 respectively. We were not able to measure ^{36}Ar and ^{38}Ar concentrations in sample Huaxi-

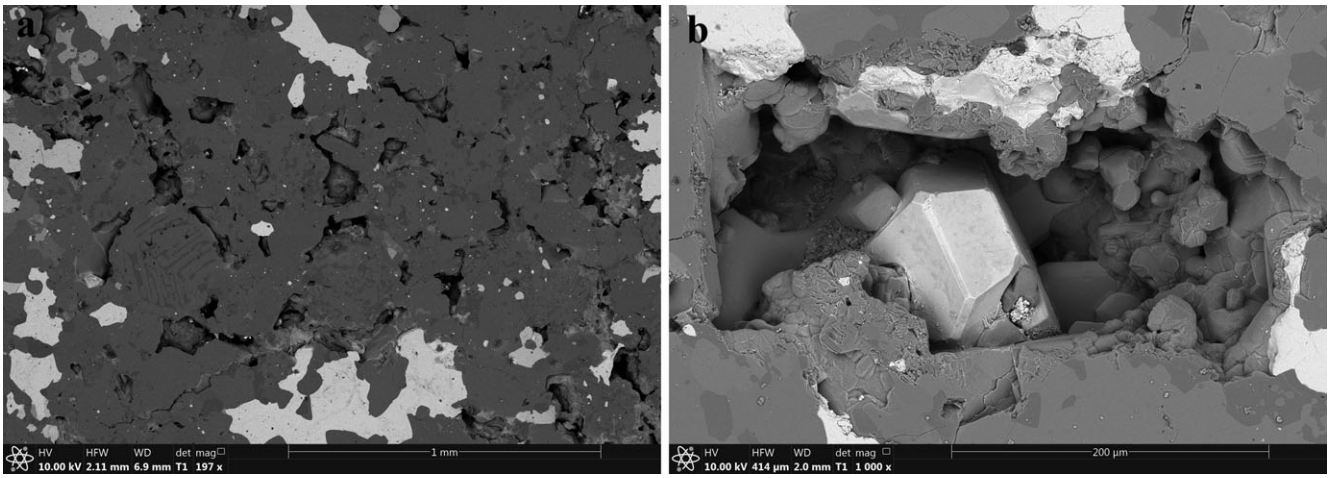

Fig. 7. Low contrast BSE images of a polished slice. a) The pores are well developed. b) The pore wall is composed of subhedron or/and isiomorphic crystals (the bright gray crystal in the middle of the pore is a troilite grain, the other crystals on the wall are silicates).

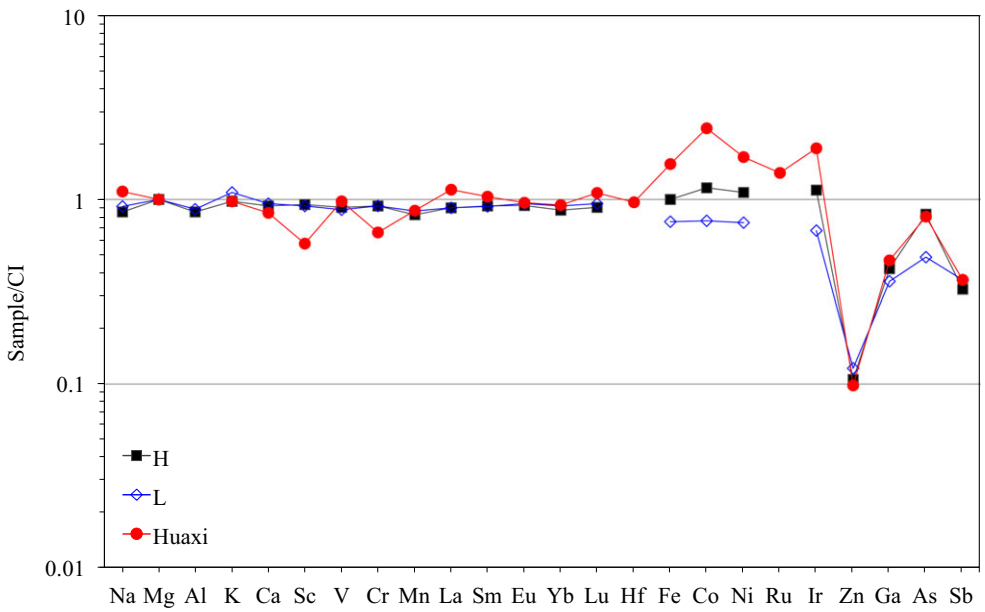

Fig. 8. Whole rock element abundances of Huaxi, H and L chondrites all normalized to Mg and CI chondrites. The CI chondrite data are from Anders and Grevesse (1989), H and L values are from Lodders and Fegley (1998). (Color figure can be viewed at wileyonlinelibrary.com.)

1 because the Ar concentrations were too low to be reliably measured. The measured ^{40}Ar concentration for Huaxi-1 is detectable because it is more than 10^4 times higher than the ^{36}Ar and ^{38}Ar concentrations. The Ar concentration and isotopic composition of the second Huaxi sample (Huaxi-2) could be measured without any problems. The $^{36}Ar/^{38}Ar$ ratio of Huaxi-2 of 3.88 indicates that the Ar is a mixture of cosmogenic and trapped. Again, considering the high petrographic grade for Huaxi we assume for the component deconvolution cosmogenic, i.e., $(^{36}Ar/^{38}Ar)_c = 0.65$, and terrestrial atmospheric contamination, i.e., $(^{36}Ar/^{38}Ar)_{air} = 5.32$, as endmembers. This decomposition yields a trapped ^{36}Ar concentration of 0.67×10^{-8}cm^{3}STP g^{-1}. The results for cosmogenic (index c) ^3He_c, $^{21}Ne_c$, $^{38}Ar_c$, and $(^{22}Ne/^{21}Ne)_c$ for Huaxi-1 and Huaxi-2 are given in Table 5. The $(^{22}Ne/^{21}Ne)_c$ ratios of the two Huaxi samples are 1.221 and 1.182, indicating relatively low preatmospheric shielding depths. Although the Ne ratios are the same within uncertainties it is the case that Huaxi-1 is located 2 mm below the fusion crust, Huaxi-2 is from about 1 cm below the fusion crust. The

Table 3. Bulk chemical composition of the Huaxi meteorite.

Element	Concentration	Unit	Method	Element	Concentration	Unit	Method
Li	1.08	μg g^{-1}	ICP-MS	Ba	1.75	μg g^{-1}	ICP-MS
Na	6473	μg g^{-1}	ICP-OES	La	312	ng g^{-1}	ICP-MS
Mg	11.6	wt%	ICP-OES	Ce	774	ng g^{-1}	ICP-MS
K	641	μg g^{-1}	ICP-OES	Pr	105	ng g^{-1}	ICP-MS
Ca	0.92	wt%	ICP-OES	Nd	512	ng g^{-1}	ICP-MS
Sc	3.93	μg g^{-1}	ICP-MS	Sm	179	ng g^{-1}	ICP-MS
V	65	μg g^{-1}	ICP-MS	Eu	63	ng g^{-1}	ICP-MS
Cr	2070	μg g^{-1}	ICP-MS	Gd	218	ng g^{-1}	ICP-MS
Mn	2036	μg g^{-1}	ICP-OES	Tb	43	ng g^{-1}	ICP-MS
Fe	34.8	wt%	ICP-AAS	Dy	239	ng g^{-1}	ICP-MS
Co	1440(*1460*)	μg g^{-1}	ICP-MS (*ICP-AAS*)	Ho	53	ng g^{-1}	ICP-MS
Ni	21992(*22700*)	μg g^{-1}	ICP-MS (*ICP-AAS*)	Er	169	ng g^{-1}	ICP-MS
Cu	85.4	μg g^{-1}	ICP-MS	Tm	30	ng g^{-1}	ICP-MS
Zn	35.9	μg g^{-1}	ICP-MS	Yb	178	ng g^{-1}	ICP-MS
Ga	5.47	μg g^{-1}	ICP-MS	Lu	31	ng g^{-1}	ICP-MS
Ge	18.1	μg g^{-1}	ICP-MS	Hf	118	ng g^{-1}	ICP-MS
As	1.76	μg g^{-1}	ICP-MS	Ta	48	ng g^{-1}	ICP-MS
Rb	1.4	μg g^{-1}	ICP-MS	Tl	0.18	ng g^{-1}	ICP-MS
Sr	10.2(*8.7*)	μg g^{-1}	ICP-MS (*ICP-OES*)	Pb	394	ng g^{-1}	ICP-MS
Y	1.72	μg g^{-1}	ICP-MS	Th	43	ng g^{-1}	ICP-MS
Zr	4.47	μg g^{-1}	ICP-MS	Ru	1164	ng g^{-1}	ICP-MS
Nb	363	ng g^{-1}	ICP-MS	Pd	987	ng g^{-1}	ICP-MS
Mo	5.35	μg g^{-1}	ICP-MS	Ir	1072	ng g^{-1}	ICP-MS
Sb	61	ng g^{-1}	ICP-MS	Pt	1780	ng g^{-1}	ICP-MS
Cs	2.74	ng g^{-1}	ICP-MS	Rh	111	ng g^{-1}	ICP-MS

The uncertainties of Na, Mg, K, Ca, Fe, Co, and Ni are lower than 0.1%, the uncertainties of trace elements are about 10%.

two Huaxi samples do differ slightly with respect to their noble gas concentrations. The $^{3}He_c$, ^{4}He, $^{21}Ne_c$, and ^{40}Ar concentrations in Huaxi-2 are ~4%, ~26%, ~3%, and ~5% higher, respectively, than the corresponding components in Huaxi-1. The differences in noble gas concentrations between both samples are most likely not due to different shielding depths but due to degassing effects during atmospheric entry. Effects like this are expected since Huaxi-1 was taken just ~2 mm below the fusion crust. The thermal history of Huaxi is discussed in more detail in the next section.

Thermal History: Helium-3/Neon-21

Figure 9 shows $(^{3}He/^{21}Ne)_c$ versus $(^{22}Ne/^{21}Ne)_c$ for Huaxi-1 and Huaxi-2, also known as a Berne plot. In addition to the experimental data we also show the empirical correlation line for chondrites as determined by Nishiizumi et al. (1980), which differs only slightly from the original one developed by Eberhardt et al. (1966). The two dashed gray lines represent the ± 15% variations from the correlation line. The black solid line represents the best fit through model calculations considering only objects with preatmospheric radii less than 65 cm and assuming ~80% ablation loss during atmospheric entry (Leya and Masarik 2009). The data for Huaxi-2 plot on the modeled correlation given by Leya and Masarik (2009) but above the empirical correlation given by Nishiizumi et al. (1980). In contrast, the data for Huaxi-1 plot below the modeled correlation but on the empirical correlation. Although we cannot exclude that the differences are due to sample inhomogneities, we rather speculate that Huaxi-1 suffered ^{3}He diffusive losses during atmospheric entry, which again is reasonable considering that this sample has been taken just ~2 mm below the fusion crust. Other possible causes, i.e., storage and preheating of the samples in the vacuum system before noble gas measurement, are very unlikely (e.g., Leya et al. 2013).

Cosmic-Ray Exposure History and Gas Retention Ages

We determined the cosmic-ray exposure (CRE) age using measured $^{3}He_c$, $^{21}Ne_c$, and $^{38}Ar_c$ concentrations and applying the correlations given by Eugster (1988) for $^{3}He_c$ versus $(^{22}Ne/^{21}Ne)_c$ and by Dalcher et al. (2013) for $^{21}Ne_c$ and $^{38}Ar_c$ versus $(^{22}Ne/^{21}Ne)_c$. Since no ^{36}Ar and ^{38}Ar could be measured for Huaxi-1, no T_{38} age has been calculated. The CRE ages based on ^{3}He (T_3) and ^{21}Ne (T_{21}) for Huaxi-1 are 1.7 ± 0.5 Ma and 2.0 ± 0.6 Ma, respectively. For Huaxi-2, T_3, T_{21}, and T_{38} ages all agree within the uncertainties, i.e.,

Table 4. Helium, Ne, and Ar concentrations (10^{-8} cm^3 STP g^{-1}) in two aliquots of Huaxi.

Sample name	Type	Mass (mg)	^3He	^4He	$^{21}Ne_c$	^{22}Ne	^{38}Ar	$^{38}Ar_c$	$^{20}Ne/^{22}Ne$	$^{21}Ne/^{22}Ne$	$(^{22}Ne/^{21}Ne)_c$	$^{36}Ar/^{38}Ar$	^{40}Ar	$^{36}Ar_{tr}$
Huaxi-1	H5	55.62	2.62 ± 0.15	1776 ± 98	0.356 ± 0.027	0.441 ± 0.033	–	–	0.912 ± 0.018	0.809 ± 0.015	1.221 ± 0.023	–	6350 ± 56	–
Huaxi-2	H5	57.09	2.73 ± 0.03	2234 ± 19	0.365 ± 0.009	0.452 ± 0.011	0.184 ± 0.008	0.055 ± 0.002	1.199 ± 0.026	0.810 ± 0.013	1.181 ± 0.020	3.88 ± 0.15	6677 ± 204	0.67 ± 0.02

Systematic uncertainties for concentrations are 3%. "c" stands for cosmogenic and "tr" stands for trapped.

Table 5. Cosmic-ray exposure ages (Ma) and gas retention ages (Ma) of Huaxi.

Sample name	Type	Mass (mg)	T_3	T_{21}	T_{38}	Adopted age (Ma)	T_4	T_{40}	T_4[a]	T_{40}[a]
Huaxi-1	H5	55.62	1.7 ± 0.5	2.0 ± 0.6		1.85 ± 0.08	4094 ± 340		4185 ± 357	
Huaxi-2	H5	57.09	1.8 ± 0.5	1.6 ± 0.5	1.5 ± 0.4	1.63 ± 0.14	4610 ± 70	4966 ± 669	4681 ± 72	4637 ± 567

Systematic uncertainties for ages are 3%.
[a]Indicates that the ages were calculated.

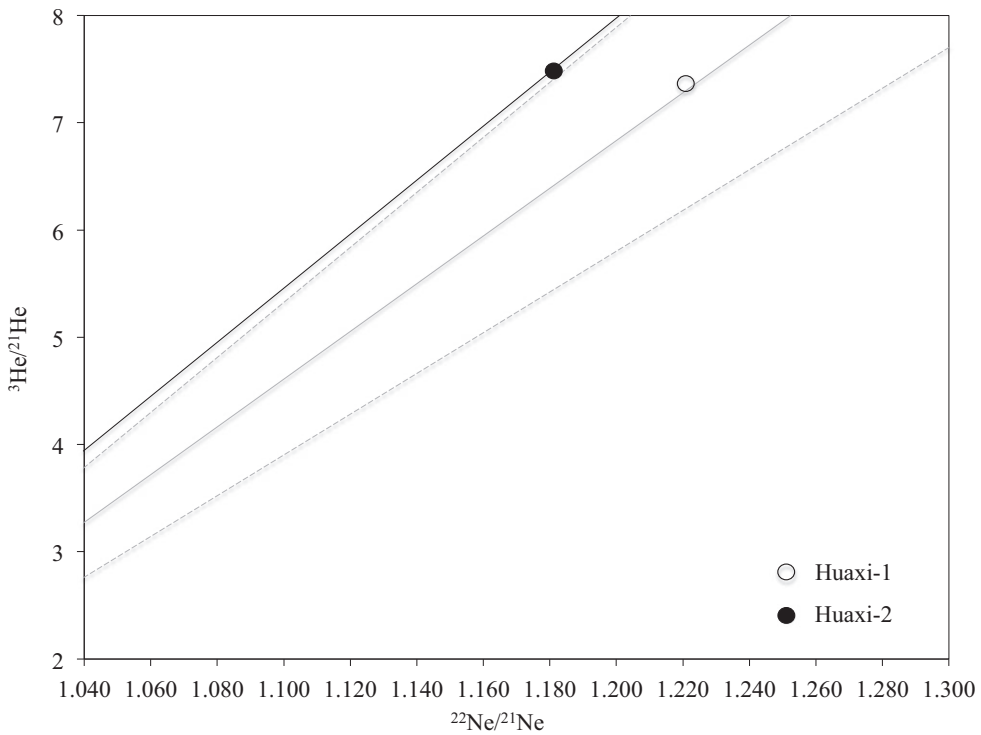

Fig. 9. Helium-3/^{21}Ne versus $^{22}Ne/^{21}Ne$ (Berne plot). In addition to the data for the two Huaxi samples the empirical correlation for chondrites given by Nishiizumi et al. (1980) is shown as a gray line. The gray dashed lines represent the ± 15% variations from the correlation. The black line represents the best fit through model calculations for ordinary chondrites with radii lower than 65 cm and assuming 80% ablation losses (Leya and Masarik 2009).

1.8 ± 0.5 Ma, 1.6 ± 0.5 Ma, and 1.5 ± 0.4 Ma, respectively. The pattern that $T_3 > T_{21} > T_{38}$ may indicates diffusive loss, but if so they are minor. We believe the results for this sample are robust and we accordingly calculate an average CRE age for Huaxi of 1.6 ± 0.1 Ma.

To calculate the ^{4}He gas retention ages (T_4) we need to subtract from the total ^{4}He concentrations the cosmogenic ^{4}He contribution. We use the relationship $(^4He/^3He)_c$ versus $(^{22}Ne/^{21}Ne)_c$ given by Leya and Masarik (2009) for H chondrites with radii of 10 cm (see below) and assume all ^{3}He to be cosmogenic. Using a Th concentration of 43 ng g^{-1} measured in bulk Huaxi and an average U concentration of 13 ng g^{-1} as given by Lodders and Fegley (1998) for H chondrites we calculated ^{4}He retention ages of 4094 Ma and

4610 Ma for Huaxi-1 and Huaxi-2, respectively. Using the average U and Th concentrations for H chondrites of Lodders and Fegley (1998) instead we obtain T_4 ages for Huaxi-1 and Huaxi-2 of 4185 Ma and 4681 Ma, respectively. Again, the short distance to the fusion crust might be the reason why T_4 for Huaxi-1 is shorter than for Huaxi-2.

Radiogenic ^{40}Ar has been calculated after removing trapped components. Using a K concentration of 641 μg g^{-1} as measured for bulk Huaxi we calculate ^{40}Ar gas retention ages (T_{40}) of 4966 Ma for Huaxi-2. However, we calculated a T_{40} age of 4637 Ma applying the average K concentration of H chondrites reported by Lodders and Fegley (1998). The K concentration measured for bulk Huaxi is slightly lower than the average K concentration for H chondrites given by Lodders and Fegley (1998), which is 780 μg g^{-1}. The T_{40} age of Huaxi-2 obtained from K concentration of 780 μg g^{-1} is about 7% lower, which is more in accord with the age of the solar system.

From the good agreement between T_3 and T_{21} and between T_4 and T_{40} for Huaxi-2 we can conclude this meteorite did not suffer He and/or Ar diffusive losses (except for ^3He and ^4He for material from close to the fusion crust), indicating that Huaxi did not experience any significant heating during its transit from the asteroid belt to Earth.

Preatmospheric Size

Meteorites enter the atmosphere at very high velocities, typically ranging from about 12 to 70 km s^{-1} (Whipple and Hughes 1955; Millman and McKinley 1963), resulting in large atmospheric friction and serious mass ablation losses. As a consequence, between 27 and 99.9% of total preatmosheric mass is lost by ablation (e.g., Bhandari et al. 1980). The average mass ablation loss of meteorites reaching Earth's surface is ~85% (Bhandari et al. 1980). Assuming symmetrical ablation losses and a one-stage CRE history we calculated the preatmospheric mass of Huaxi using the empirical relation between preatmospheric masses and $(^{22}Ne/^{21}Ne)_c$ given by Bhandari et al. (1980). Doing so, we calculate a preatmospheric mass of Huaxi of ~21 kg with a radius of ~11 cm, based on a bulk density of 3.21 g cm^{-3} measured in this study.

SUMMARY AND CONCLUSIONS

Petrographical and mineralogical investigations of Huaxi indicate that it belongs to the H5 ordinary chondrite group; a classification confirmed by the data for bulk chemical composition and grain density. Undulose extinction; rareness of irregular fractures; and the absence of planar fracture in olivine, low-Ca pyroxene, and plagioclase grains imply that Huaxi suffered only very weak shock metamorphism (S2). Huaxi has a high porosity of 17.6%, which could be a consequence of the low shock stage.

The preatmospheric mass of Huaxi was ~21 kg with a preatmospheric radius of ~11 cm. This meteorite has a relatively short cosmic-ray exposure age of 1.6 ± 0.1 Ma and long T_4 and T_{40} gas retention ages of ~ 4681 and ~ 4637 Ma, respectively.

Acknowledgments—This work was supported by the National Natural Science Foundation of China (grants 41273080, 41473067, and 41490630). We acknowledge the journalists Yao Wu and Jing Sun from Guizhou TV for providing us the information of the Huaxi meteorite fall. We thank Mr. Zhou for providing sample material. We are grateful to Guy Consolmagno and Yangting Lin for constructive reviews, and thank Associate Editor Marc Caffee for his editorial efforts and valuable suggestions. In addition, we thank the engineer Wenqin Zheng from the Institute of Geochemistry, Chinese Academy of Sciences, for her help during the mineralogical and chemical studies and Hans-Erich Jenni for his support during the noble gas measurements.

Editorial Handling—Dr. Marc Caffee

REFERENCES

Ammon K., Masarik J., and Leya I. 2008. Noble gases in Grant and Carbo and the influence of S- and P-rich mineral inclusions on the ^{41}K-^{40}K dating system. *Meteoritics & Planetary Science* 43:685–699.

Anders E. and Grevesse N. 1989. Abundances of the elements: Meteoric and solar. *Geochimica et Cosmochimica Acta* 53:197–214.

Bhandari N., Lal D., Rajan R. S., Arnold J. R., Marti K., and Moore C. B. 1980. Atmospheric ablation in meteorites: A study based on cosmic ray tracks and neon isotopes. *Nuclear Tracks* 4:213–262.

Choi B. G., Kim H., Kim H., Lee J. I., Kim T. H., Ahn I., Yi K., and Hong T. E. 2015. Jinju H5 chondrite: a new fall in Korea having numerous vugs filled with vapor-phase crystallized minerals (abstract #5091). 78th Annual Meeting of the Meteoritical Society. Meteoritics & Planetary Science 50.

Consolmagno S., Macke S., Rochette P., Britt D. T., and Gattacceca J. 2006. Density, magnetic susceptibility, and the characterization of ordinary chondrite falls and showers. *Meteoritics & Planetary Science* 41:331–342.

Consolmagno G. J., Britt D. T., and Macke R. J. 2008. The significance of meteorite density and porosity. *Chemie der Erde* 68:1–29.

Dalcher N., Caffee M. W., Nishiizumi K., Welten K. C., Vogel N., Wieler R., and Leya I. 2013. Calibration of cosmogenic noble gas production in ordinary chondrites

based on ^{36}Cl-^{36}Ar ages. Part 1: Refined produced rate for cosmogenic ^{21}Ne and ^{38}Ar. *Meteoritics & Planetary Science* 48:1841–1862.

Eberhardt P., Eugster O., Geiss J., and Marti K. 1966. Rare gas measurements in 30 stone meteorites. *Zeitschrift für Naturforschung Teil A* 21:414–426.

Eugster O. 1988. Cosmic-ray production rates for ^{3}He, ^{21}Ne, ^{38}Ar, ^{83}Kr, and ^{126}Xe in chondrites based on ^{81}Kr-Kr ages. *Geochimica et Cosmochimia Acta* 52:1649–1662.

Friedrich J. M., Rubin A. E., Beard S. P., Swindle T. D., Isachsen C. E., Rivers M. L., and Macke R. J. 2014. Ancient porosity preserved in ordinary chondrites: Examining shock and compaction on young asteroids. *Meteoritics & Planetary Science* 49:1214–1231.

Gomes C. B. and Keil K. 1980. *Brazilian stone meteorites*. Albuquerque, New Mexico: University of New Mexico Press.

Keil K. and Fredriksson K. 1964. The Fe, Mg and Ca distribution in coexisting olivines and rhombic pyroxenes of chondrites. *Journal of Geophysical Research* 69:3487–3515.

Leya I. and Masarik J. 2009. Cosmogenic nuclides in stony meteorites revisited. *Meteoritics & Planetary Science* 44:1061–1086.

Leya I., Ammon K., Cosarinsky M., Dalcher N., Gnos E., Hofmann B., and Huber L. 2013. Light noble gases in 12 meteorites from the Omani desert, Australia, Mauritania, Canada, and Sweden. *Meteoritics & Planetary Science* 48:1401–1414.

Li S. J., Wang S. J., Li X. Y., Li Y., Liu S., and Coulson I. M. 2012. A new method for the measurement of meteorite bulk volume via ideal gas pycnometry. *Journal of Geophysical Research* 117:E10001.

Lodders K. and Fegley B. Jr. 1998. *The planetary scientist's companion*. New York: Oxford University Press. 371 p.

Macke R. J. 2010. Survey of meteorite physical properties: Density, porosity and magnetic susceptibility. Ph.D. thesis, University of Central Florida, Orlando, Florida, USA.

Millman P. M. and McKinley D. W. R. 1963. Meteors. In *The solar system IV: The Moon, meteorites and comets*, edited by Middlehurst B. M. and Kuiper G. P. Chicago: University of Chicago. pp. 674–773.

Nishiizumi K., Regnier S., and Marti K. 1980. Cosmic ray exposure ages of chondrites, pre-irradiation and constancy of cosmic ray flux in the past. *Earth and Planetary Science Letters* 50:156–170.

Qi L., Gregoire D. C., Zhou M. F., and Malpas J. 2003. Determination of Pt, Pd, Ru and Ir in geological samples by ID-ICP-MS using sodium peroxide fusion and Te co-precipitation. *Geochemical Journal* 37:557–565.

Qi L., Gao J., Huang X., Hu J., Zhou M. F., and Zhong H. 2011. An improved digestion technique for determination of platinum group elements in geological samples. *Journal of Analytical Atomic Spectrometry* 26:1900–1904.

Ruzicka A., Grossman J. N., and Garvie L. 2014. The Meteoritical Bulletin, No. 100. *Meteoritics & Planetary Science* 49:E1–E101.

Sasso M. R., Macke R. J., Boesenberg J. S., Britt D. T., Rivers M. L., Ebel D. S., and Friedrich J. M. 2009. Incompletely compacted equilibrated ordinary chondrites. *Meteoritics & Planetary Science* 44:1743–1753.

Stöffler D., Keil K., and Scott E. R. D. 1991. Shock metamorphism of ordinary chondrites. *Geochimica et Cosmochimica Acta* 55:3845–3867.

Van Schmus W. R. and Wood J. A. A. 1967. Chemical-petrologic classification for the chondritic meteorites. *Geochimica et Cosmochimica Acta* 31:747–765.

Whipple F. L. and Hughes R. F. 1955. On the velocities and orbits of meteors, fireballs and meteorites. In *Meteors*, edited by Kaizer T. R. London: Pergamon Press. pp. 149–156.

Wlotzka F. 1993. A weathering scale for the ordinary chondrites. *Meteoritics* 28:460.